Characterizing Feshbach resonances in ultracold scattering calculations

Matthew D. Frye and Jeremy M. Hutson*
Joint Quantum Centre (JQC) Durham-Newcastle, Department of Chemistry, Durham University, South Road, Durham DH1 3LE, United Kingdom
(Received 15 August 2017; published 11 October 2017)

We describe procedures for converging on and characterizing zero-energy Feshbach resonances that appear in scattering lengths for ultracold atomic and molecular collisions as a function of an external field. The elastic procedure is appropriate for purely elastic scattering, where the scattering length is real and displays a true pole. The regularized scattering length procedure is appropriate when there is weak background inelasticity, so that the scattering length is complex and displays an oscillation rather than a pole, but the resonant scattering length $a_{\rm res}$ is close to real. The fully complex procedure is appropriate when there is substantial background inelasticity and the real and imaginary parts of $a_{\rm res}$ are required. We demonstrate these procedures for scattering of ultracold ^{85}Rb in various initial states. All of them can converge on and provide full characterization of resonances, from initial guesses many thousands of widths away, using scattering calculations at only about ten values of the external field.

DOI: 10.1103/PhysRevA.96.042705

I. INTRODUCTION

Zero-energy Feshbach resonances are formed when a bound or quasibound state is tuned across a threshold by varying an applied field, most commonly a magnetic field. They are ubiquitous in studies of ultracold physics [1], where they can be used to tune scattering lengths for many applications, including studies of equations of state [2], solitons [3], and Efimov physics [4,5]. They are also used for magnetoassociation to form ultracold molecules [6,7].

Low-energy scattering may be described by the energy-dependent scattering length $a(E,B) = -k^{-1}\tan\delta$, where $E = \hbar^2k^2/2\mu$ is the collision energy, μ is the reduced mass, and δ is the scattering phase shift. This is constant as $E \to 0$, where it reduces to the usual zero-energy scattering length. At constant energy it is convenient to write $a(E,B)$ as simply $a(B)$. In the simplest case of an isolated narrow resonance without inelastic scattering, $a(B)$ is real and shows a simple pole as a function of applied field B. If the background scattering length $a_{\rm bg}(B)$ is constant across the width of the resonance, the pole is described by [8]

$$a(B) = a_{\rm bg}\left(1 - \frac{\Delta}{B - B_{\rm res}}\right), \tag{1}$$

where $B_{\rm res}$ is the position of the resonance, and the width of the resonance is characterized by Δ. The parameters are generally weakly dependent on energy in the threshold region. Obtaining them from quantum scattering calculations based on interaction potentials is an important problem in ultracold collision physics.

It is possible to locate both the pole and the zero of the scattering length and converge on them numerically using standard root-finding algorithms [9,10]. In the case where $a_{\rm bg}(B)$ is constant, Δ is the separation between the pole and the zero. For resonances that are not isolated and narrow, the behavior of the scattering length is more complicated than Eq. (1). Nevertheless, Eq. (1) always holds in some region close to the pole and the parameters may be defined in terms of this local behavior. When this is done, $a_{\rm bg}$ may not describe $a(B)$ far from the pole and Δ may not be precisely the separation between the pole and a zero. Such effects are particularly prominent when there are numerous overlapping resonances [11] or when $a_{\rm bg}$ is small so that the zero is artificially far from the pole [12].

If inelastic decay is present then the scattering length is complex [13] and its behavior is considerably more complicated. It has no clearly defined zero crossing and it no longer shows a pole but instead oscillates with a finite amplitude [14,15]. This may render decayed resonances unsuitable for tuning scattering lengths to large values [16]. In addition, inelastic rates usually peak sharply near resonance [17] and the resulting losses may make the resonances unsuitable for purposes such as magnetoassociation [18]. In other cases, Feshbach resonances can actually *reduce* inelastic cross sections, which might aid sympathetic cooling [15,19].

In the inelastic case, there is no efficient procedure available to locate and characterize Feshbach resonances. It is in principle possible to obtain resonance parameters by explicit least-squares fitting of S-matrix elements from quantum scattering calculations to appropriate functional forms [20]. It is also possible to extract an overall width by fitting to the S-matrix eigenphase sum as a function of energy [20]. This approach has been used for zero-energy Feshbach resonances as a function of magnetic field [17,19], but it requires large numbers of scattering calculations and substantial manual labor. Better methods are clearly needed.

In this paper we describe efficient, automatable procedures for locating and characterizing zero-energy Feshbach resonances, both in the purely elastic case and in the presence of inelastic scattering. Our algorithms are built on an approach for resonances in purely elastic scattering that we have used previously [12,21] but have not described in detail. This converges towards a pole using an iterative three-point fit to calculated scattering lengths. We begin by describing an improved algorithm for this case that converges stably on widths and background scattering lengths as well as pole positions. We then extend the approach to handle the important case when there is inelastic scattering but the inelastic loss away from resonance is small. Finally, we deal with the case where there is strong background inelastic scattering. All the methods have been implemented in the general-purpose

*j.m.hutson@durham.ac.uk

quantum scattering package MOLSCAT [22] and are illustrated here with examples from calculations on collisions of ^{85}Rb [23].

II. ELASTIC SCATTERING

We first describe a reliable general method for converging on and characterizing a resonance in the case of purely elastic scattering. Early versions of this method have been employed in previous work [12,21], but here we refine it and provide a complete description. We refer to the method described in this section as the elastic procedure.

The elastic procedure uses three calculated scattering lengths a_1, a_2, and a_3 at fields B_1, B_2, and B_3, respectively, close to the resonance. Solving three simultaneous equations allows us to extract the three parameters from Eq. (1). Defining

$$\rho = \left(\frac{B_3 - B_1}{B_2 - B_1}\right)\left(\frac{a_2 - a_1}{a_3 - a_1}\right), \tag{2}$$

we obtain

$$B_{\rm res} = \frac{B_3 - B_2\rho}{1 - \rho}, \tag{3}$$

$$a_{\rm bg}\Delta = \frac{(B_3 - B_{\rm res})(B_1 - B_{\rm res})(a_3 - a_1)}{B_3 - B_1}, \tag{4}$$

and finally

$$a_{\rm bg} = a_1 + \frac{a_{\rm bg}\Delta}{B_1 - B_{\rm res}}. \tag{5}$$

In order to iterate and converge towards the pole we must not only choose a point for a new scattering calculation but also choose which of the previous three results to discard. The obvious choice for a new point is the estimated $B_{\rm res}$, but this causes points to pile up close to the pole, and Eqs. (2)–(5) are numerically unstable when two points are very close together. We therefore choose the new point with the aim that the final three points should include one point very close to the pole, one point between $t_{\rm min}\Delta$ and $2t_{\rm min}\Delta$ from the pole, and one point between $t_{\rm max}\Delta$ and $2t_{\rm max}\Delta$ from the pole on the opposite side. These three points can be thought of as allowing characterization of $B_{\rm res}$, $a_{\rm bg}\Delta$, and $a_{\rm bg}$, respectively. The tolerances $t_{\rm min}$ and $t_{\rm max}$ are positive, with $t_{\rm min} < t_{\rm max}$. The values $t_{\rm min} = 0.1$ and $t_{\rm max} = 1.0$ are almost always appropriate for isolated resonances; we use these values throughout this paper, but different choices may be appropriate in other cases. We terminate the iteration when the estimated value of $B_{\rm res}$ is within a small amount ϵ of the closest of the three points and the other two points satisfy the criteria above. The logic we have implemented to select which point to discard and where to place the next point is shown in Fig. 1.

We need three fields in the vicinity of the resonance to start the procedure. We choose to use equally spaced points separated by a small amount δB; in this work we choose this value to be 0.2 G. The algorithm will, of course, perform best when one of the initial points is close to the pole, but in this paper we choose points such that the pole is approximately at the midpoint of two of them to provide the strictest test of the procedure. In practice, the initial estimate of the pole position could come from a number of different sources such as scattering calculations on a grid or calculations of the bound states of the system; we usually use the program FIELD [24], which can directly calculate fields at which there is a bound state exactly at threshold.

To demonstrate the convergence of this method, we apply it to a resonance near 171 G in collisions of two ^{85}Rb atoms in their lowest $(F = 2, M_F = 2)$ state. Scattering lengths are calculated using the MOLSCAT package, as described by Blackley *et al.* [23], at energy $E = 1\ {\rm nK} \times k_{\rm B}$. We choose $\epsilon = 10^{-9}$ G, which is limited by noise in our scattering calculations. Table I summarizes the convergence towards the resonance, with the parameters estimated by Eqs. (2)–(5) at each iteration; Fig. 2 provides a graphical representation of the convergence process. This resonance is narrow, with $\Delta = 2.3 \times 10^{-5}$ G, yet our method successfully converges rapidly on the pole even though the closest of the three initial points is over 4000 widths away. The eighth and ninth points are actually placed away from the pole by the algorithm to satisfy the requirements associated with $t_{\rm min}$ and $t_{\rm max}$ before the final point is placed extremely close to the pole. The entire procedure needs only ten scattering calculations and requires no human intervention after the initial set of points; a corresponding manual search and subsequent least-squares fit would have needed many more scattering calculations and considerable human input.

If the pole position $B_{\rm res}$ is all that is required, and Δ and $a_{\rm bg}$ are unimportant, then the fastest convergence is often achieved by setting $t_{\rm min} = t_{\rm max} = 0$. With this choice, the present algorithm reduces to that used in previous work from our group [12,21]. The equations for Δ and $a_{\rm bg}$ then become unstable as convergence proceeds and the points cluster close to the pole, but $B_{\rm res}$ usually converges smoothly.

All the algorithms described here make the approximation that $a_{\rm bg}(B)$ is constant across the range of points. This approximation improves as the convergence proceeds and the range of points becomes smaller. Nevertheless, it is the limiting factor that determines the distance from which convergence can be achieved. At least one of the initial points must give a scattering length that is affected by the resonance by more than the variation of $a_{\rm bg}(B)$ across the range of the points. For very narrow resonances, computational noise in the scattering length can also affect convergence.

III. INELASTIC SCATTERING

In the presence of inelastic loss, the diagonal S-matrix element in the incoming channel $S_{00} = \exp(2i\delta)$ has magnitude less than 1. The phase shift δ is thus complex, and so is the scattering length $a = \alpha - i\beta$, where $\beta \geqslant 0$ [13]. The real and imaginary parts of the scattering length characterize the elastic and inelastic cross sections, respectively. The energy-dependent scattering length may be written exactly as [14]

$$a(E,B) = \frac{-\tan\delta(E,B)}{k} = \frac{1}{ik}\left(\frac{1 - S_{00}(E,B)}{1 + S_{00}(E,B)}\right). \tag{6}$$

Around a resonance, the scattering length at constant energy describes a circle in the complex plane [14], beginning and ending at the background scattering length $a_{\rm bg}$,

$$a(B) = a_{\rm bg} + \frac{a_{\rm res}}{2(B - B_{\rm res})/\,\Gamma_B^{\rm inel} + i}. \tag{7}$$

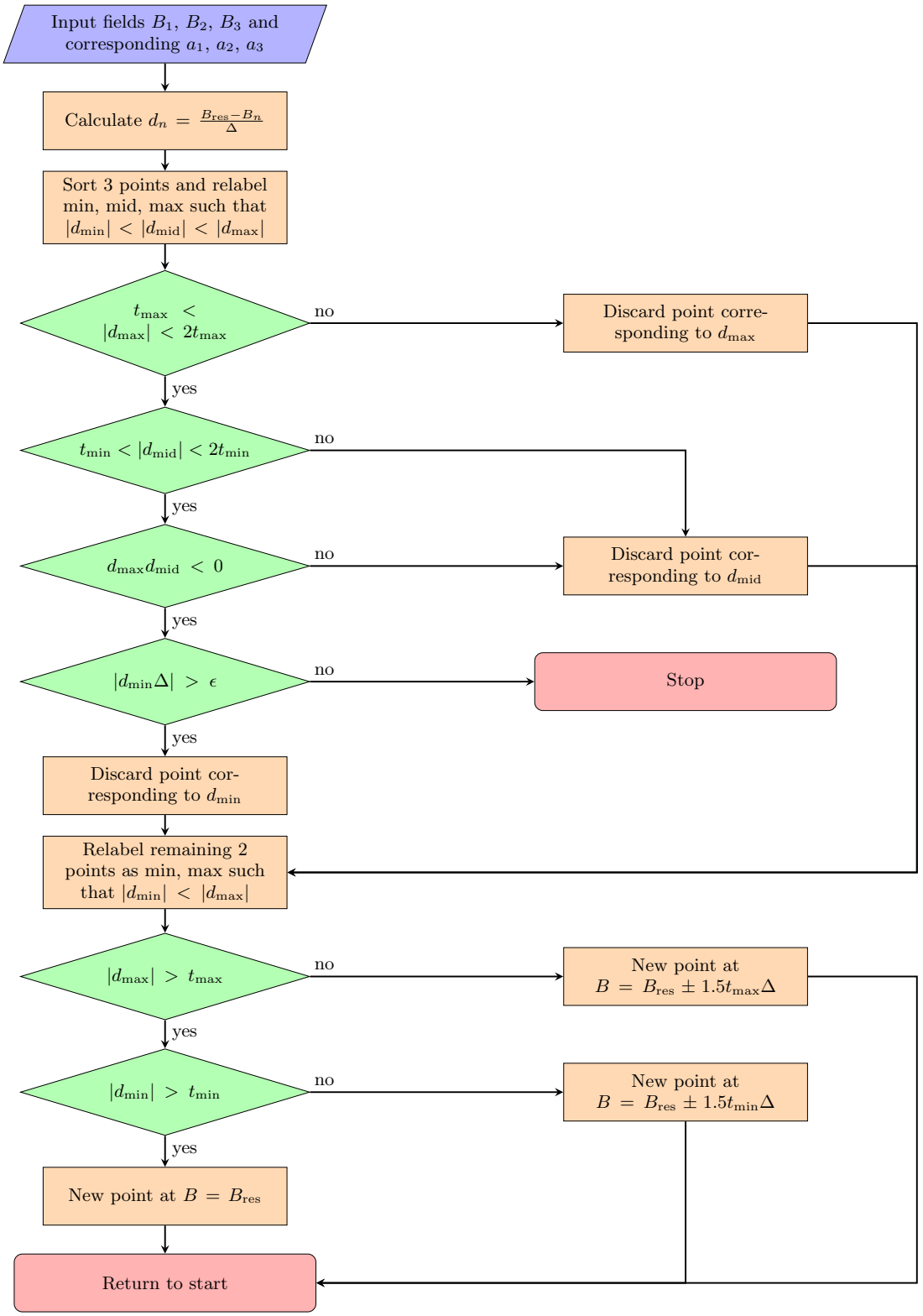

FIG. 1. Flowchart representation of the algorithm to select which point to discard and where to place the next point.

$a_{\rm bg} = \alpha_{\rm bg} - i\beta_{\rm bg}$ is now complex and $a_{\rm res} = \alpha_{\rm res} - i\beta_{\rm res}$ is a resonant scattering length that describes the size and direction of the circle. In addition, $\Gamma_B^{\rm inel}$ is a decay width for the quasibound state that causes the resonance; it is a real quantity, with dimensions of field whose sign depends on the magnetic moment of the state relative to the threshold. It is useful to identify

$$\alpha_{\rm res}\Gamma_B^{\rm inel} = -2\alpha_{\rm bg}\Delta \tag{8}$$

to allow a connection back to Eq. (1), although Δ no longer has a simple interpretation as the distance between the pole and zero in a.

TABLE I. Convergence towards the resonance near $B_{\rm ref} = 171.561$ G for two ^{85}Rb atoms in their $F = 2, M_F = 2$ state. Units are G and the Bohr radius a_0.

	Resonance near $B_{\rm ref} = 171.561$ G						
				Estimated values			
n	$B_n - B_{\rm ref}$	$(B_n - B_{\rm res})/\Delta$	a	$B_{\rm res} - B_{\rm ref}$	Δ	$a_{\rm bg}$	$a_{\rm bg}\Delta$
1	-1.00227×10^{-1}	4.24×10^{3}	-438.67				
2	2.99773×10^{-1}	-1.27×10^{4}	-438.76				
3	9.97730×10^{-2}	-4.24×10^{3}	-438.85	3.40045×10^{-2}	-1.8427×10^{-5}	-438.73	8.0846×10^{-3}
4	3.40045×10^{-2}	-1.45×10^{3}	-439.06	3.68297×10^{-3}	-2.0840×10^{-5}	-438.75	9.1437×10^{-3}
5	3.68297×10^{-3}	-166	-441.40	-3.79856×10^{-4}	-2.4633×10^{-5}	-438.74	1.0807×10^{-2}
6	-3.79856×10^{-4}	6.49	-371.13	-2.26739×10^{-4}	-2.3598×10^{-5}	-438.75	1.0354×10^{-2}
7	-2.26739×10^{-4}	-0.00989	-44657	-2.26973×10^{-4}	-2.3563×10^{-5}	-438.76	1.0339×10^{-2}
8	-2.23438×10^{-4}	-0.150	-3364.4	-2.26973×10^{-4}	-2.3568×10^{-5}	-438.77	1.0341×10^{-2}
9	-2.62324×10^{-4}	1.50	-146.31	-2.26973×10^{-4}	-2.3565×10^{-5}	-438.82	1.0341×10^{-2}
10	-2.26973×10^{-4}	4.24×10^{-5}	1.631×10^{7}	-2.26972×10^{-4}	-2.3564×10^{-5}	-438.76	1.0339×10^{-2}

Around a decayed resonance, both α and β show an oscillation, determined by $a_{\rm res}$, rather than a pole [14,15,19]. This has implications for the observation and use of such resonances [16–18]. In the very common case $|a_{\rm res}| \gg \beta_{\rm bg}$, $\beta(B)$ displays a peak of magnitude $a_{\rm res}$. However, $a_{\rm res}$ is *inversely* proportional to $\Gamma_B^{\rm inel}$. Somewhat counterintuitively, therefore, *weaker* inelastic decay of the quasibound state responsible for the resonance causes a *higher* peak in $\beta(B)$ (and hence in the inelastic rate) around $B_{\rm res}$.

A. Weak background inelasticity

We first consider the important case where the background inelasticity can be neglected, so we approximate $\beta_{\rm bg} = 0$. Under this approximation $a_{\rm res}$ is real [19], though $a(B)$ itself remains complex near resonance. There are thus only four parameters to extract. Even so, Eq. (7) does not allow us to extract parameters as easily as we could from Eq. (1). However, this can be overcome by defining a regularized scattering length

$$\mathcal{A} = \alpha + \frac{\beta^2}{\alpha - \alpha_{\rm bg}} \tag{9}$$

$$= \alpha_{\rm bg} - \frac{\alpha_{\rm bg}\Delta}{B - B_{\rm res}}, \tag{10}$$

which is real and shows a simple pole just like Eq. (1). This allows us to use Eqs. (2)–(5) with a replaced by $\mathcal{A}$ to extract three of the parameters and converge on the resonance position as before, with minimal modification of the elastic procedure. We refer to the resulting method as the regularized scattering length (RSL) procedure.

The final parameter $a_{\rm res}$ can be estimated at each stage of the convergence using the identity

$$a_{\rm res} = \frac{|a - a_{\rm bg}|^2}{\beta} = \beta + \frac{(\alpha - \alpha_{\rm bg})^2}{\beta}. \tag{11}$$

In the important case where $\Gamma_B^{\rm inel}$ is very small, the peak in β is very narrow. Estimating $a_{\rm res}$ from the maximum value of β can thus be very difficult, but Eq. (11) provides a useful estimate as soon as both α and β differ significantly from their background values. Equations (9) and (11) each needs an estimate of $\alpha_{\rm bg}$. This can be obtained iteratively, but we find that in practice it is adequate to take it from the previous or current iteration, respectively. To calculate $\mathcal{A}$ at the first iteration we use the average of a_1 and a_2 as an initial approximation for $a_{\rm bg}$. Equation (11) can also be used separately from the convergence algorithm employed here, for example, to estimate $a_{\rm res}$ from scattering calculations on a grid that is not fine enough to resolve the peak in β.

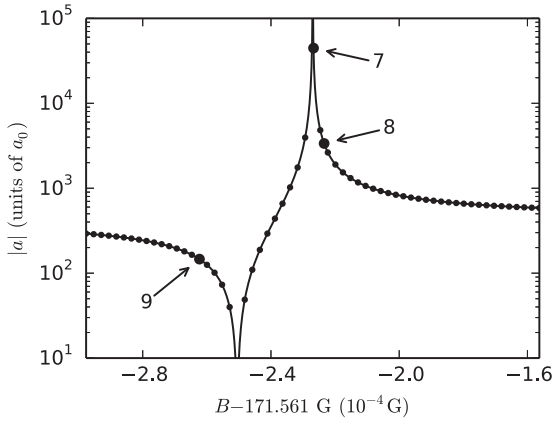

FIG. 2. Convergence towards the elastic resonance near 171 G for two ^{85}Rb atoms in their $F = 2, M_F = 2$ state. Note the logarithmic vertical scale. The closed circles show $|a|$ from scattering calculations at the sequence of points n produced by the elastic procedure, the black line shows Eq. (1) with the final estimated parameters, and the small dots show the results of scattering calculations on a grid for comparison.

Table II summarizes the convergence towards two resonances in collisions of a pair of ^{85}Rb atoms in their $F = 2$, $M_F = -2$ excited state, using the RSL procedure. These results are also shown in Fig. 3. These collisions are weakly inelastic away from resonances, because loss comes only from spin-relaxation transitions driven by the weak dipole-dipole interaction. We use a slightly larger value for the convergence criterion than in the previous section, $\epsilon = 10^{-8}$ G.

The first inelastic resonance we analyze, near 215 G, shows only weak inelastic decay, as seen from the small values

TABLE II. Convergence towards resonances with weak background inelasticity for two ^{85}Rb atoms in their $F = 2, M_F = -2$ state. Units are G and the Bohr radius a_0.

	Resonance near $B_{\rm ref} = 215.084$ G								
						Estimated values			
n	$B_n - B_{\rm ref}$	$(B_n - B_{\rm res})/\Delta$	α_n	β_n	$\mathcal{A}_n$	$B_{\rm res} - B_{\rm ref}$	Δ	$a_{\rm bg}$	$a_{\rm res}$
1	-9.96246×10^{-2}	-18.0	-402.1	0.000796	-402.1				
2	3.00375×10^{-1}	53.9	-374.5	0.000692	-374.5				
3	1.00375×10^{-1}	18.0	-360.0	0.000649	-360.0	2.81284×10^{-3}	5.514×10^{-3}	-381.53	7.168×10^{5}
4	2.81284×10^{-3}	0.438	489.6	0.00219	489.6	3.95129×10^{-4}	5.524×10^{-3}	-381.02	3.459×10^{8}
5	3.95129×10^{-4}	0.00354	1.07×10^{5}	67.6	1.07×10^{5}	3.75429×10^{-4}	5.568×10^{-3}	-381.19	1.716×10^{8}
6	-7.97622×10^{-3}	-1.50	-635.1	0.00197	-635.1	3.75433×10^{-4}	5.569×10^{-3}	-381.01	1.716×10^{8}
7	1.21083×10^{-3}	0.150	2159	0.0299	2159	3.75433×10^{-4}	5.569×10^{-3}	-381.00	1.716×10^{8}
8	3.75433×10^{-4}	-1.80×10^{-7}	-1.32×10^{7}	1.70×10^{8}	-2.19×10^{9}	3.75434×10^{-4}	5.569×10^{-3}	-381.00	1.707×10^{8}
	Resonance near $B_{\rm ref} = 603.977$ G								
1	-9.93851×10^{-2}	-531	-476.7	0.00159	-476.7				-
2	3.00615×10^{-1}	1.59×10^{3}	-475.6	1.39×10^{-5}	-475.6				-
3	1.00615×10^{-1}	531	-475.0	0.000630	-475.0	1.08784×10^{-2}	1.7996×10^{-4}	-475.91	1.446×10^{3}
4	1.08784×10^{-2}	54.5	-467.1	0.0954	-467.1	9.67212×10^{-4}	1.8191×10^{-4}	-475.82	7.991×10^{2}
5	9.67212×10^{-4}	1.87	-246.8	76.3	-221.4	6.13682×10^{-4}	1.8905×10^{-4}	-475.86	7.635×10^{2}
6	6.13682×10^{-4}	-0.00659	-483.8	762	-7.32×10^{4}	6.14914×10^{-4}	1.8838×10^{-4}	-475.82	7.621×10^{2}
7	5.86657×10^{-4}	-0.150	-648.9	720	-3647	6.14919×10^{-4}	1.8837×10^{-4}	-475.81	7.621×10^{2}
8	6.14919×10^{-4}	-2.65×10^{-5}	-475.8	762	-1.84×10^{7}	6.14924×10^{-4}	1.8838×10^{-4}	-475.83	7.621×10^{2}

of β and negligible differences between α and $\mathcal{A}$ except at the final point. The RSL procedure converges smoothly and provides stable values of all the resonance parameters. The fitted $\beta(B)$ is shown in Fig. 3(a); it is accurate near the center of the resonance, but deviates from the calculated values by a small amount in the wings because the actual background $\beta_{\rm bg}$ is nonzero. As described above, the RSL procedure provides an estimate $a_{\rm res} = 1.7 \times 10^8 a_0$ that is stable over the final few iterations even when β is six orders of magnitude smaller than $a_{\rm res}$; the final calculation confirms that these estimates of $a_{\rm res}$ are remarkably accurate. For this resonance, the elastic procedure would work well until the last point, when it would predict a pole position some distance away from the resonance. The elastic procedure would thus fail to converge, and continue indefinitely, repeatedly approaching the resonance and jumping away again.

The second resonance we analyze, near 604 G, is quite strongly decayed. The pole in α is strongly suppressed, to the point that α does not even cross zero. By contrast, the regularized scattering length still has a pole and zero crossing as before. The elastic procedure would fail completely anywhere near the center of the resonance, but with the modification of Eq. (9) we can efficiently converge to the resonance position. The final fitted $\alpha(B)$ and $\beta(B)$, shown in Fig. 3(b), agree very well with the calculated values, demonstrating that the resonance has been accurately characterized. The new fitted value of $\Delta = 1.8 \times 10^{-4}$ G is two orders of magnitude smaller than the value reported previously [23], which was obtained by fitting $\alpha(B)$ to Eq. (1) far from resonance.

B. Strong background inelasticity

Finally, we consider the case with background inelasticity included. There are now six parameters required to characterize a resonance according to Eq. (7): $B_{\rm res}$, $\Gamma_B^{\rm inel}$, and the real and imaginary parts of $a_{\rm bg}$ and $a_{\rm res}$. However, each value of $a(B)$ has real and imaginary parts, so we again need scattering calculations at only three fields.

We begin by locating the scattering length at the center of the circle described by Eq. (7), $a_{\rm c} = a_{\rm bg} - i a_{\rm res}/2$. Starting from the equation for a circle, $(\alpha_n - \alpha_{\rm c})^2 + (\beta_n - \beta_{\rm c})^2 = R^2$, it is straightforward to derive the simultaneous equations

$$\begin{pmatrix} \alpha_2 - \alpha_1 & \beta_2 - \beta_1 \\ \alpha_3 - \alpha_2 & \beta_3 - \beta_2 \end{pmatrix} \begin{pmatrix} \alpha_{\rm c} \\ \beta_{\rm c} \end{pmatrix} = \frac{1}{2} \begin{pmatrix} |a_2|^2 - |a_1|^2 \\ |a_3|^2 - |a_2|^2 \end{pmatrix}. \tag{12}$$

These are solved to obtain $a_{\rm c}$ and $R = |a_n - a_{\rm c}| = |a_{\rm res}|/2$. Across the resonance, the angle θ around this circle is described by a Breit-Wigner phase

$$\frac{\theta}{2} = \frac{\theta_{\rm bg}}{2} + \arctan\left(\frac{\Gamma^{\rm inel}}{2(B_{\rm res} - B)}\right). \tag{13}$$

We define the dimensionless quantity

$$\widetilde{a}(B) = \tan\frac{\theta}{2} = \tan\left(\frac{\arg[a(B) - a_{\rm c}]}{2}\right), \tag{14}$$

which has a pole analogous to Eq. (1). We evaluate $\widetilde{a}_1$, $\widetilde{a}_2$, and $\widetilde{a}_3$ at B_1, B_2, and B_3 and use Eqs. (2)–(5) to obtain parameters $\widetilde{B}_{\rm res}$, $\widetilde{\Delta}$, and $\widetilde{a}_{\rm bg}$ (which do not have immediate physical interpretations). Now $\widetilde{a}_{\rm bg} = \tan(\theta_{\rm bg}/2)$ tells us where $a_{\rm bg}$ lies on the circle,

$$a_{\rm bg} = a_{\rm c} + R\exp(i\theta_{\rm bg}), \tag{15}$$

and therefore

$$a_{\rm res} = 2i(a_{\rm c} - a_{\rm bg}). \tag{16}$$

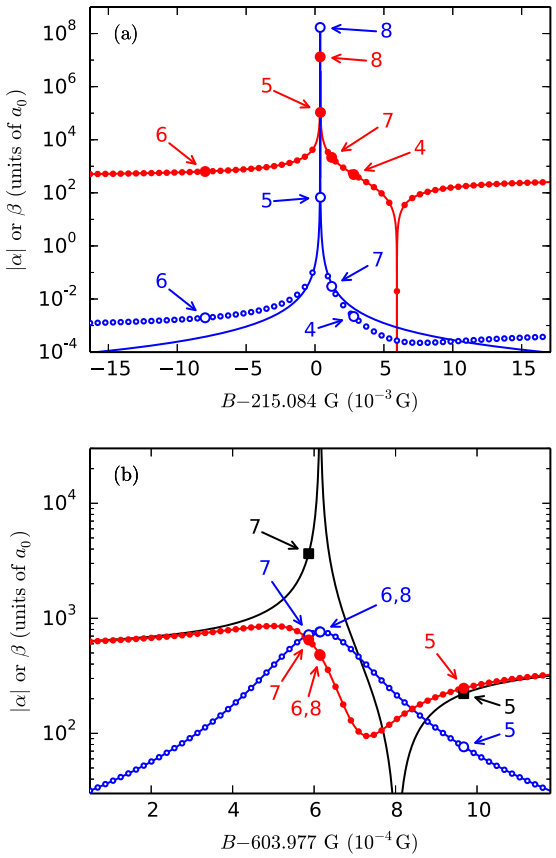

FIG. 3. Convergence towards resonances with weak background inelasticity for two ^{85}Rb atoms in their $F = 2, M_F = -2$ state: (a) resonance near 215 G and (b) resonance near 604 G. The large symbols show values of $|\alpha|$ (red closed circles) and β (blue open circles) from scattering calculations at the sequence of points n produced by the RSL procedure, the fitted functions are shown as corresponding lines through the symbols, and the small dots show the results of scattering calculations on a grid for comparison. The black squares and line in (b) show the regularized scattering length $\mathcal{A}$.

Since $a(B_{\rm res})$ is diametrically opposite $a_{\rm bg}$ on the circle,

$$\widetilde{a}(B_{\rm res}) = \tan\left(\frac{\theta_{\rm bg}+\pi}{2}\right) = -\frac{1}{\widetilde{a}_{\rm bg}}. \tag{17}$$

We then obtain $B_{\rm res}$ from

$$B_{\rm res} = \widetilde{B}_{\rm res} - \frac{\widetilde{a}_{\rm bg}\widetilde{\Delta}}{\widetilde{a}(B_{\rm res}) - \widetilde{a}_{\rm bg}} = \widetilde{B}_{\rm res} + \frac{\widetilde{\Delta}}{1+\widetilde{a}_{\rm bg}^{-2}}. \tag{18}$$

Finally, we obtain $\Gamma_B^{\rm inel}$ from one calculated scattering length using Eq. (7).

This procedure provides an estimate of $B_{\rm res}$ and other parameters from calculations of $a(B)$ at a set of three points. We iterate using the algorithm described in Sec. II, but using the larger of $\Gamma_B^{\rm inel}$ and Δ to constrain the separation of the points from $B_{\rm res}$. We refer to the resulting method as the fully complex procedure.

To demonstrate this, we consider convergence towards a resonance near 172 G in collisions of two ^{85}Rb atoms in their $F = 3, M_F = 2$ excited state. In this case the atoms can decay through spin-exchange collisions, which cause faster inelastic loss away from resonance than in Sec. III A. The convergence is summarized in Table III and shown in Fig. 4, using $\epsilon = 10^{-7}$ G. The procedure converges rapidly on the resonance position and the final fitted functions show excellent agreement with the calculated scattering lengths. The resonance is very strongly decayed; $|a_{\rm res}|$ is less than $5a_0$ and has a substantial imaginary component. This makes the oscillations in $\alpha(B)$ and $\beta(B)$ somewhat asymmetric.

The fully complex procedure can also resolve the discrepancy between the calculated $\beta(B)$ and the fitted function far from resonance in Fig. 3(a). Figure 5 shows the results of the fully complex procedure in this case, and it may be seen that excellent agreement is obtained. The converged values of the parameters are very similar to those in Table II, with the addition of $\beta_{\rm bg} = 7.20 \times 10^{-4} a_0$ and $\beta_{\rm res} = -582 a_0$.

For this procedure to converge well, the circle in the complex plane described by $a(B)$ must be well formed. Variation of $a_{\rm bg}(B)$ across the width of the resonance can distort the circle; if this distortion is significant compared to the size of the circle, the procedure may fail. This leads to the criterion

$$\left|\frac{da_{\rm bg}}{dB}\Gamma_B^{\rm inel}\right| \ll |a_{\rm res}|. \tag{19}$$

The procedure may thus be unsuitable for the widest and most strongly decayed resonances (large $\Gamma_B^{\rm inel}$ and small $a_{\rm res}$). The procedure may also fail for overlapping resonances. These

TABLE III. Convergence towards the resonance near $B_{\rm ref} = 171.845$ G for two ^{85}Rb atoms in their $F = 3, M_F = 2$ state. Units are G and the Bohr radius a_0.

	Resonance near $B_{\rm ref} = 171.845$ G									
					Estimated values					
n	$B_n - B_{\rm ref}$	$(B_n - B_{\rm res})/\Delta$	α_n	β_n	$B_{\rm res} - B_{\rm ref}$	$\Gamma_B^{\rm inel}$	$\alpha_{\rm bg}$	$\beta_{\rm bg}$	$\alpha_{\rm res}$	$\beta_{\rm res}$
1	-1.00244×10^{-1}	38.0	−490.99	22.388						
2	2.99756×10^{-1}	−114	−491.02	22.371						
3	9.97560×10^{-2}	−38.0	−491.09	22.386	6.92055×10^{-2}	-4.7788×10^{-2}	−491.01	22.377	0.10979	0.065852
4	6.92055×10^{-2}	−26.4	−491.12	22.391	1.58950×10^{-2}	-1.2632×10^{-2}	−491.03	22.384	0.71330	0.026746
5	1.58950×10^{-2}	−6.14	−491.40	22.446	-2.91246×10^{-3}	-1.5078×10^{-3}	−491.01	22.376	9.7150	−1.3474
6	-2.91246×10^{-3}	1.01	−489.17	23.122	-1.80823×10^{-4}	-2.7312×10^{-3}	−491.03	22.382	4.4502	−0.37429
7	-1.80823×10^{-4}	−0.0241	−490.88	26.918	-2.43111×10^{-4}	-2.6270×10^{-3}	−491.04	22.386	4.5243	−0.36788
8	1.50937×10^{-4}	−0.150	−491.94	26.638	-2.44221×10^{-4}	-2.6291×10^{-3}	−491.04	22.387	4.5232	−0.37363
9	-2.44221×10^{-4}	1.75×10^{-6}	−490.67	26.910	-2.44216×10^{-4}	-2.6290×10^{-3}	−491.04	22.387	4.5232	−0.37361

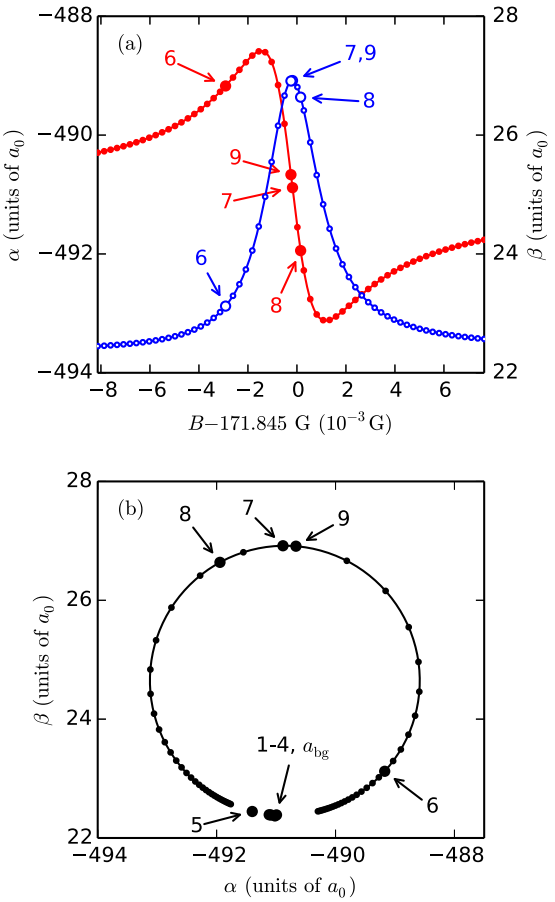

FIG. 4. Convergence towards the resonance near 172 G for two ^{85}Rb atoms in their $F = 3, M_F = 2$ state. (a) α (red closed circles) and β (blue open circles) from scattering calculations at the sequence of points n produced by the fully complex procedure. The fitted functions are shown as corresponding lines through the symbols and the small dots show the results of scattering calculations on a grid for comparison. (b) Circle described by $a(B) = \alpha(B) - i\beta(B)$ in the complex plane.

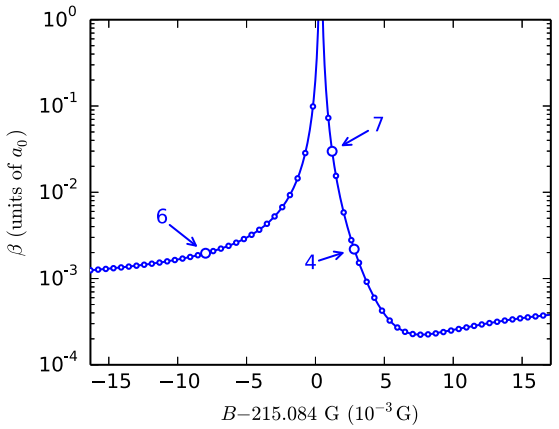

FIG. 5. Convergence towards the resonance near 215 G for two ^{85}Rb atoms in their $F = 2, M_F = -2$ state using the fully complex procedure. Only β is shown and the axis is expanded to show the asymmetry clearly. Symbols and lines are as in previous figures.

restrictions are similar to the criteria used to define an isolated narrow resonance [20,25].

IV. CONCLUSION

In this paper we have developed three procedures for efficiently and accurately converging on and characterizing different kinds of zero-energy Feshbach resonances as a function of external field. These procedures can converge on and accurately characterize resonances, from initial guesses many thousands of widths away, with a total of only around ten scattering calculations.

First we described the elastic procedure. This is designed for resonances in purely elastic scattering, where the scattering length has a true pole. At each iteration, the procedure characterizes the resonance using scattering calculations at three values of the external field while ensuring that the points do not cluster too close to the pole. This allows stable evaluation of the width and background scattering length as well as the pole position.

For the case of weak background inelasticity we have developed the regularized scattering length procedure. The oscillation in the complex scattering length is converted into a true pole in a regularized scattering length, and convergence on the pole is achieved in the same way as in the elastic procedure. We also provided a means to estimate the resonant scattering length a_{res} from calculations in the wings of the resonance.

Finally, we have developed a fully complex procedure to converge on and extract all six parameters needed to characterize resonances when there is substantial background inelasticity and the real and imaginary parts of a_{bg} and a_{res} are required.

ACKNOWLEDGMENTS

The authors are grateful to C. R. Le Sueur for valuable discussions on implementation of these procedures in the MOLSCAT program. This work has been supported by the UK Engineering and Physical Sciences Research Council (Grant No. EP/I012044/1).

[1] C. Chin, R. Grimm, E. Tiesinga, and P. S. Julienne, Feshbach resonances in ultracold gases, Rev. Mod. Phys. **82**, 1225 (2010).

[2] S. Nascimbène, N. Navon, F. Chevy, and C. Salomon, The equation of state of ultracold Bose and Fermi gases: A few examples, New J. Phys. **12**, 103026 (2010).

[3] D. J. Frantzeskakis, Dark solitons in atomic Bose-Einstein condensates: From theory to experiments, J. Phys. A **43**, 213001 (2010).

[4] T. Kraemer, M. Mark, P. Waldburger, J. G. Danzl, C. Chin, B. Engeser, A. D. Lange, K. Pilch, A. Jaakkola, H. C. Nägerl, and R. Grimm, Evidence for Efimov quantum states in an

ultracold gas of caesium atoms, Nature (London) **440**, 315 (2006).

[5] B. Huang, L. A. Sidorenkov, R. Grimm, and J. M. Hutson, Observation of the Second Triatomic Resonance in Efimov's Scenario, Phys. Rev. Lett. **112**, 190401 (2014).

[6] J. M. Hutson and P. Soldán, Molecule formation in ultracold atomic gases, Int. Rev. Phys. Chem. **25**, 497 (2006).

[7] T. Köhler, K. Góral, and P. S. Julienne, Production of cold molecules via magnetically tunable Feshbach resonances, Rev. Mod. Phys. **78**, 1311 (2006).

[8] A. J. Moerdijk, B. J. Verhaar, and A. Axelsson, Resonances in ultracold collisions of ^{6}Li, ^{7}Li, and ^{23}Na, Phys. Rev. A **51**, 4852 (1995).

[9] D. A. Brue and J. M. Hutson, Magnetically Tunable Feshbach Resonances in Ultracold Li-Yb Mixtures, Phys. Rev. Lett. **108**, 043201 (2012).

[10] T. Takekoshi, M. Debatin, R. Rameshan, F. Ferlaino, R. Grimm, H.-C. Nägerl, C. R. Le Sueur, J. M. Hutson, P. S. Julienne, S. Kotochigova, and E. Tiemann, Towards the production of ultracold ground-state RbCs molecules: Feshbach resonances, weakly bound states, and coupled-channel models, Phys. Rev. A **85**, 032506 (2012).

[11] K. Jachymski and P. S. Julienne, Analytical model of overlapping Feshbach resonances, Phys. Rev. A **88**, 052701 (2013).

[12] H.-W. Cho, D. J. McCarron, M. P. Köppinger, D. L. Jenkin, K. L. Butler, P. S. Julienne, C. L. Blackley, C. R. Le Sueur, J. M. Hutson, and S. L. Cornish, Feshbach spectroscopy of an ultracold mixture of ^{85}Rb and ^{133}Cs, Phys. Rev. A **87**, 010703(R) (2013).

[13] N. Balakrishnan, V. Kharchenko, R. C. Forrey, and A. Dalgarno, Complex scattering lengths in multi-channel atom-molecule collisions, Chem. Phys. Lett. **280**, 5 (1997).

[14] J. M. Hutson, Feshbach resonances in the presence of inelastic scattering: Threshold behavior and suppression of poles in scattering lengths, New J. Phys. **9**, 152 (2007). Note that there is a typographical error in Eq. (22) of this paper: The last term on the right-hand side should read $-\beta_{\rm res}$ instead of $+\beta_{\rm res}$.

[15] J. M. Hutson, M. Beyene, and M. L. González-Martínez, Dramatic Reductions in Inelastic Cross Sections for Ultracold Collisions Near Feshbach Resonances, Phys. Rev. Lett. **103**, 163201 (2009).

[16] J. L. Bohn and P. S. Julienne, Prospects for influencing scattering lengths with far-off-resonant light, Phys. Rev. A **56**, 1486 (1997).

[17] M. L. González-Martínez and J. M. Hutson, Ultracold atom-molecule collisions and bound states in magnetic fields: Zero-energy Feshbach resonances in He-NH ($^3\Sigma^-$), Phys. Rev. A **75**, 022702 (2007).

[18] M. L. González-Martínez and J. M. Hutson, Magnetically tunable Feshbach resonances in Li + Yb(^3P_J), Phys. Rev. A **88**, 020701(R) (2013).

[19] R. A. Rowlands, M. L. González-Martínez, and J. M. Hutson, Ultracold collisions in magnetic fields: Reducing inelastic cross sections near Feshbach resonances in He-NH, arXiv:0707.4397.

[20] C. J. Ashton, M. S. Child, and J. M. Hutson, Rotational predissociation of the Ar-HCl van der Waals complex: Close-coupled scattering calculations, J. Chem. Phys. **78**, 4025 (1983).

[21] G. Zürn, T. Lompe, A. N. Wenz, S. Jochim, P. S. Julienne, and J. M. Hutson, Precise Characterization of ^{6}Li Feshbach Resonances Using Trap-Sideband-Resolved rf Spectroscopy of Weakly Bound Molecules, Phys. Rev. Lett. **110**, 135301 (2013).

[22] J. M. Hutson and C. R. Le Sueur, MOLSCAT computer program, 2017.

[23] C. L. Blackley, C. R. Le Sueur, J. M. Hutson, D. J. McCarron, M. P. Köppinger, H.-W. Cho, D. L. Jenkin, and S. L. Cornish, Feshbach resonances in ultracold ^{85}Rb, Phys. Rev. A **87**, 033611 (2013).

[24] J. M. Hutson, FIELD computer program, version 1, 2011.

[25] C. J. Ashton, Predissociation and scattering resonances in atom-diatom systems, Ph.D. thesis, Oxford University, 1981.